CHEMISTRY OF MATERIALS
Article

Chem. Mater. **2010,** *22,* 409–413 409
DOI:10.1021/cm902825c

Iron(III)-oxo Centers on TiO_2 for Visible-Light Photocatalysis

Joseph A. Libera,[†] Jeffrey W. Elam,[†] Norman F. Sather,[†] Tijana Rajh,[‡] and Nada M. Dimitrijevic*[,‡,§]

[†]*Energy Systems Division,* [‡]*Center for Nanoscale Materials, and* [§]*Chemical Sciences and Engineering Division, Argonne National Laboratory, Argonne, Illinois 60439*

Received September 9, 2009. Revised Manuscript Received November 25, 2009

Isolated iron(III)-oxo clusters were synthesized onto TiO_2 using atomic layer deposition. The Fe_xO_y/TiO_2 nanocomposites have unique properties that enable not only absorption of visible light, but efficient photocatalysis as demonstrated by methylene blue degradation. The localization of photogenerated electrons in core TiO_2 nanocrystallites upon visible light excitation demonstrates coupling of conduction bands of mixed oxides. The redox properties of photogenerated charges in nanocomposites were studied using in situ electron paramagnetic resonance spectroscopy.

Introduction

The design and development of TiO_2 photocatalysts that are able to utilize not only UV but also visible or solar light irradiation has been pursued for decades.[1] Chemical doping of TiO_2 with nitrogen (p-type doping) or transition metals (n-type doping), although shifting the bandgap to lower values, yields varying success in catalytic performance using visible light. Namely, it has been shown that the states introduced by nitrogen doping lie closely above the valence band edge of TiO_2 promoting absorption in visible.[2,3] However, two types of nitrogen states are created, interstitial sites that favor carrier recombination, and the substitutional sites that promote visible-light photocatalysis, the relative abundance of the two nitrogen-doping species depends on the preparation conditions.[4] On the other hand, chemical doping with transition metals creates almost exclusively impurity energy levels that decrease photocatalytic efficiency dramatically even under UV irradiation because of the quick recombination of the photogenerated charges. The improvement in visible light photocatalysis was obtained when TiO_2 was bombarded with hig-energy transition metal ions such as V, Cr, Mn, Fe, and Ni resulting in the modification of the electronic properties of bulk TiO_2 photocatalysts because of the creation of transition metal substitutional sites in titania lattice.[1] Creating transition metal oxo-centers on the surface of TiO_2 can provide alternative approach for the synthesis of titania-based nanocomposites that utilize visible-light photocatalysis. Namely, the work of Frei[5,6] and Anpo[7] on the isolated metal-oxo species in zeolite and MCM-41 cages shows that such species can act both as light-harvesting and catalytic centers.

In this paper, we are reporting on the photocatalytic properties of Fe_xO_y centers created on the surface of TiO_2 (Degussa P25) using Atomic Layer Deposition (ALD). ALD is a thin film growth technique uniquely capable of depositing both highly conformal metal oxide layers on nanostructured materials, as well as highly dispersed and uniform submonolayer deposits on porous substrates for catalytic applications.[8−10] We have chosen ferric oxide type centers because: (i) iron is abundant and cheap, (ii) Fe^{3+} centers greatly enhance catalytic activity of oxide substrates,[11] and (iii) the nonstochiometric Fe_xO_y clusters, if isolated on titania surface, are expected to promote coupling of band edges of mixed composite, and thus charge separation.[12] Ferric oxide (α-Fe_2O_3, or hematite) by itself absorbs a large part of the solar spectrum; however, its use in photocatalysis is limited mainly because of the short hole diffusion length,[13] and different strategies are applied to minimize the distance photogenerated holes have to diffuse to reach the Fe_2O_3/electrolyte interface while still allowing for efficient light absorption.[14,15] Additionally, the

*Corresponding author. E-mail: dimitrijevic@anl.gov.

(1) Anpo, M. Bull. Chem. Soc. Jpn. **2004**, *77*, 1427, and references cited therein.
(2) Asahi, R.; Morikawa, T.; Ohwaki, T.; Aoki, K.; Taga, Y. *Science* **2001**, *293*, 269.
(3) Lindgren, T.; Mwabora, J. M.; Avendano, E.; Jonsson, J.; Hoel, A.; Granqvist, C.-G.; Lindquist, S.-E. *J. Phys. Chem. B* **2003**, *107*, 5709.
(4) Di Valentin, C.; Pacchioni, G.; Selloni, A.; Livraghi, S.; Giamello, E. *J. Phys. Chem. B* **2005**, *109*, 11414.
(5) Lin, W.; Frei, H. *J. Am. Chem. Soc.* **2005**, *127*, 1610.
(6) Han, H.; Frei, H. *Microporous Mesoporous Mater.* **2007**, *103*, 265.
(7) Anpo, M.; Thomas, J. M. *Chem. Commun.* **2006**, 3273.
(8) Ritala, M.; Leskela, M. Atomic Layer Deposition. In *Handbook of Thin Film Materials*; Nalwa, H. S., Ed.; Academic Press: San Diego, 2001; Vol. *1*; p 103.
(9) Haukka, S.; Lakomaa, E. L.; Suntola, T. Adsorption controlled preparation of heterogeneous catalysts. In *Adsorption and Its Applications in Industry and Environmental Protection, Vol I: Applications in Industry*; Studies in Surface Science and Catalysis; Elsevier: New York, 1999; Vol. *120*, pp 715−750.
(10) Libera, J. A.; Elam, J. W.; Pellin, M. J. *Thin Solid Films* **2008**, *516*, 6158.
(11) Parmaliana, A.; Arena, F; Frusteri, F.; Martinez-Arias, A.; Lopez Granados, M.; Fierro, J. L. G. *Appl. Catal. A* **2002**, *226*, 163.
(12) Liu, H.; Gao, L. *J. Am. Ceram. Soc.* **2006**, *89*, 370.
(13) Kennedy, J. H.; Frese, K. W. *J. Electrochem. Soc.* **1978**, *125*, 709.
(14) Kay, A.; Cesar, I.; Gratzel, M. *J. Am. Chem. Soc.* **2006**, *128*, 15714.
(15) Cesar, I.; Kay, A.; Martinez, J. A. G.; Gratzel, M. *J. Am. Chem. Soc.* **2006**, *128*, 4582.

Published on Web 12/30/2009

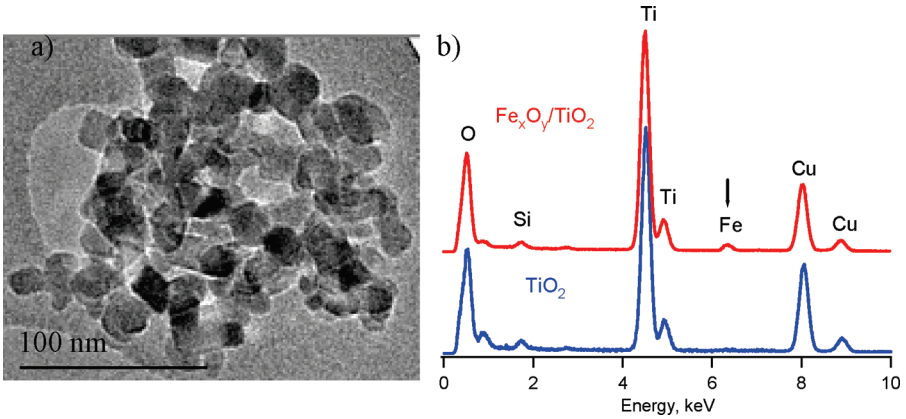

Figure 1. (a) Transmission electron microscopy and (b) energy-dispersive X-ray spectra of Fe_xO_y/TiO_2.

position of conduction band edge of 0.28 V makes hematite a relatively inefficient reducing agent.

Experimental Section

Materials Synthesis. The Fe_xO_y ALD was performed using a viscous flow reactor as described previously.[10,16] Approximately 100 mg of Degussa P25 Aeroxide was placed in a thin layer in a stainless steel tray. A gas permeable cover was used to secure the contents of the tray inside the ALD reactor during the deposition. The ALD reactor temperature was 200 °C. Iron Tris(2,2,6,6-tetramethyl-3,5-heptanedionate), $Fe(thd)_3$, was delivered by passing the carrier gas through a vessel containing the reactant maintained at 135 °C. Reactants were introduced into the reactor using continuously flowing ultrahigh purity (99.999%) nitrogen as the carrier gas at a flow rate of 360 sccm and a pressure of 1 Torr. Each ALD cycle consisted of (a) 300 s exposure to $Fe(thd)_3$, (b) 150 s purge, (c) 150 s ozone exposure, and (d) 150 s purge. A total of four cycles were applied to the P25 powder. This treatment should produce an iron oxide coating with an average thickness of ~0.5 Å.[17] The long exposures were necessary to ensure infiltration of the reactants to the high surface area of the P25 powder. No additional thermal treatments were performed.

The synthesis and characterization of 6.5 nm α-Fe_2O_3 colloidal particles was according to published procedure.[18] The mixture of 0.5% Fe_2O_3 with TiO_2 (Fe_2O_3/TiO_2) was prepared by combining a colloidal solution of iron oxide with TiO_2 (P25) and further heating it at 150 °C for 18 h.

Techniques. The samples were characterized by transmission electron microscopy (TEM, JEOL 100CX) energy-dispersive X-ray spectroscopy (EDS), and UV/vis reflectance spectroscopy (Beckman DU 640 spectrometer).

Electron paramagnetic resonance (EPR) spectra were collected on a Bruker Elexys E580 spectrometer equipped with a helium cryostat. For the characterization of photogenerated charges, samples dispersed in Milli-Q water were purged with argon, and illuminated within the cavity while spectra were acquired. The EPR spectra were recorded both at cryogenic and room temperatures. For reaction of photogenerated charges with spin trap TEMPO free radical (2,2,6,6-tetramethylpiperidine 1-oxyl), the measurements were obtained at room temperature in an aerated aqueous solution containing 20 μM TEMPO. A 300 W xenon lamp (ILC Inc.) was used as the light source for EPR studies. The *g* tensor values were calibrated for homogeneity and accuracy by comparing to a coal standard ($g = 2.00285 \pm 0.00005$).

The photodegradation of methylene blue (MB) was carried out in a 50 mL glass reactor, with continuous stirring, using a 300 W Xe lamp as a light source. The water filter was used as a cut off for IR light. The photocatalysts were dispersed in aqueous solution in a concentration of 2 mg/mL, the MB concentration was 10 mM. At time intervals of illumination, 200 μL aliquots were centrifuged at 10 krpm and absorption spectra of supernatant were measured using Shimatzu 1601 UV/vis spectrometer.

In this work, we used 420 nm cutoff filter in various experiments to prevent excitation of rutile phase of Degussa P25, and refer in text to wavelengths $\lambda > 420$ nm as "visible light".

Results and Discussion

Characterization of Nanocomposites. The ALD of iron oxide onto surface of TiO_2 did not affect the primary morphology or aggregation state of nanocrystals to any appreciable extent. Figure 1a shows the typical TEM image of the ALD Fe_xO_y/TiO_2. The aggregates are characteristic of TiO_2 Degussa P25, and no difference in size or morphology can be observed for samples before and after ALD. The elemental analysis carried out in EDS experiments, Figure 1b, has confirmed the presence of Fe on the surface of TiO_2, the estimated value being (0.5 ± 0.1) % by atom. The existence and identity of iron species in the synthesized nanocomposites was further investigated with more sensitive techniques, including UV−visible and EPR spectroscopies.

The diffuse reflectance spectrum of Fe_xO_y/TiO_2 nanocomposites is presented in Figure 2. The complexity of the spectrum arises from the presence of different Fe(III) species, from isolated to clustered. Deconvulation of spectrum (dashed line) into subbands indicates various ligand-to-metal charge transfer (CT) transitions, the $t_1 \rightarrow t_2$ and $t_1 \rightarrow e$ being characteristic of a Fe^{3+} ions.[19] For isolated Fe(III), CT transitions give rise to bands below 300 nm, whereas CT bands between 300 and 400 nm are

(16) Elam, J. W.; Groner, M. D.; George, S. M. *Rev. Sci. Instrum.* **2002**, *73*, 2981.
(17) Lie, M.; Fjellvag, H.; Kjekshus, A. *Thin Solid Films* **2005**, *488*, 74.
(18) Chen, L. X.; Liu, T.; Thurnauer, M. C.; Csencsits, R.; Rajh, T. *J. Phys. Chem. B* **2002**, *106*, 8539.
(19) Tippins, H. H. *Phys. Rev. B* **1970**, *1*, 126.

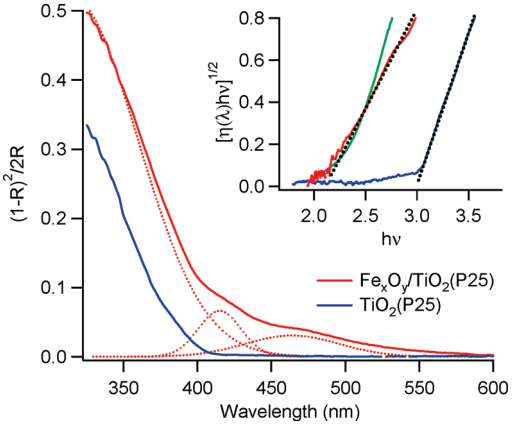

Figure 2. Diffuse reflectance spectra of core TiO_2 and Fe_xO_y/TiO_2 nanocomposite. The *y*-axis is expressed in Kubelka−Munk units (R = reflectance). Inset shows the band gap of TiO_2 and Fe_xO_y/TiO_2 obtained from the intercept of $[\eta(\lambda)h\nu]^{1/2}$ vs $h\nu$ for indirect transition. The green line corresponds to physical mixture Fe_2O_3/TiO_2.

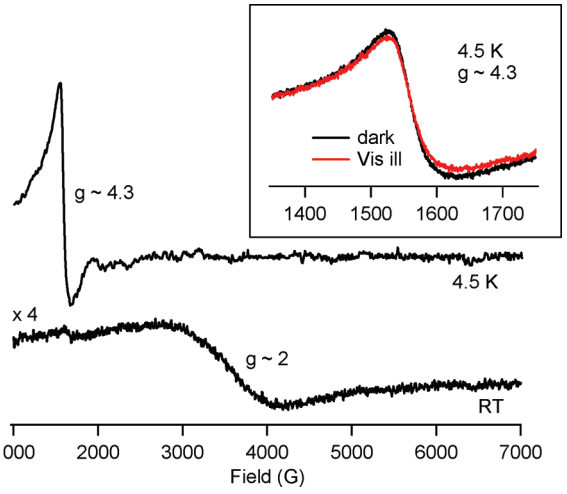

Figure 3. EPR spectra of Fe_xO_y/TiO_2 nanocomposites measured at 4.5 K and at room temperature. Inset: low-field EPR spectra measured at 4.5 K in dark, black line, and under visible-light illumination (Xe-lamp, cut off filter 420 nm), red line.

generally assigned to octahedral Fe(III) in small oligomeric Fe_xO_y clusters,[20] and those above 450 nm to larger Fe_2O_3 particles.[21]

The value for bandgap (E_g) was extrapolated assuming indirect transition (Figure 2, inset), as both TiO_2 and ferric oxides are indirect semiconductors.[22] The presence of iron-oxo centers on the surface of TiO_2 shifts the bandgap from 3.0 eV for TiO_2 P25 to 2.1 eV, the value very close to the bandgap of Fe_2O_3 (E_g = 2.0−2.2 eV).[23]

EPR Spectroscopy of Photogenerated Charges in Nanocomposites. The presence of isolated Fe(III)-oxo clusters in nanocomposites was confirmed by EPR spectroscopy. The X-band spectra of Fe_xO_y/TiO_2 measured at 4.5 and 293 K are presented in Figure 3. The spectrum measured at 4.5 K revealed a strong signal with g-tensor value $g_{eff} \approx 4.3$ indicating presence of isolated Fe^{3+} ions predominantly situated in rhombically distorted octahedral or tetrahedral oxygen environments.[24−26] The dominance of isolated iron(III)-oxo centers (Fe_xO_y) in nanocomposites is further confirmed by the absence of signal at $g \approx 2.0$ at 4.5 K which arises from superexchange interaction between the iron ions in close proximity, i.e., in large Fe_2O_3 clusters, resulting in so-called superparamagnetic resonance.[25] The very weak and broad signal appears only when temperature is raised to 293 K. In general, EPR spectra of Fe^{3+} ions chemically deposited in oxide glasses and on solids are characterized by the appearance of both resonance absorptions $g \approx 4.3$ and $g \approx 2.0$ at a low temperature of 4 K. The relative intensities of two signals strongly depend on the composition, the intensity of a signal associated with large clusters increases with the concentration of ferric oxide/hydroxide. Furthermore, the shape of signal associated with isolated Fe(III)-oxo centers is almost temperature independent, whereas the superparamagnetic resonance signal increases in intensity and narrows as temperature increases.[25] Thus, the absence of a signal at $g \approx 2.0$ at 4.5 K and its large broadening at 293 K suggests very low concentration of large clusters (Fe_2O_3) in the ALD Fe_xO_y/TiO_2 nanocomposites.

Low-temperature EPR was further employed to examine the initial separation of photogenerated charges upon illumination with visible light. Illuminating Fe_xO_y/TiO_2 nanocomposites by visible light ($\lambda_{exc} > 420$ nm) results in the slight decay of a signal associated with isolated Fe(III)-oxo centers (Fe_xO_y), indicating that they, probably together with larger clusters, participate in light-induced charge formation (Figure 3, inset). The decrease in the intensity of Fe^{3+} signal upon illumination is a result of localization of photogenerated electrons on iron and subsequent formation of Fe^{2+} nonparamagnetic ions; however, the decrease is much smaller than for a physical mixture of Fe_2O_3/TiO_2 or hematite alone. Consequently, the EPR has revealed localization of photogenerated electrons into the bulk of core material (TiO_2). The signals from both lattice trapped electrons in rutile ($g_\perp = 1.975$)[27] and anatase ($g_\perp = 1.990$)[28] crystallites were observed upon visible light excitation at 4.5 K, Figure 4, red line. For comparison, the EPR spectra of bare TiO_2 P25 under UV (black line), and visible light (blue line) illumination are also presented in Figure 4. When bare titania nanoparticles are excited with $\lambda > 420$ nm, there is not enough energy to excite electrons from the valence to the conduction band, thus no signal from photogenerated charges can be observed. At the same time, no EPR signals

(20) Bordiga, S.; Buzzoni, R.; Geobaldo, F.; Lamberti, C.; Giamello, E.; Zecchina, A.; Leofanti, G.; Petrini, G.; Tozzola, G.; Vlaic, G. *J. Catal.* **1996**, *158*, 486.
(21) Kumar, S. M.; Schwidder, M.; Grunert, W.; Bruckner, A. *J. Catal.* **2004**, *227*, 384.
(22) Pankove, J. I. *Optical Processes in Semiconductors*; Prentice-Hall: Englewood Cliffs, NJ, 1971.
(23) Xu, Y.; Schoonen, M. A. A. *Am. Mineral.* **2000**, *85*, 543.
(24) Komastu, T.; Soga, N. *J. Chem. Phys.* **1980**, *72*, 1781.
(25) Bergera, R.; Bisseya, J.-C.; Kliava, J.; Daubric, H.; Estournes, C. *J. Magn. Magn. Mater.* **2001**, *234*, 535.
(26) Singh, R. K.; Kothiyal, G. P.; Srinivasan, A. *Solid State Commun.* **2008**, *146*, 25.
(27) Hurum, D. C.; Agrios, A. G.; Gray, K. A.; Rajh, T.; Thurnauer, M. C. *J. Phys. Chem. B* **2003**, *107*, 4545.
(28) (a) Howe, R. F.; Graetzel, M. *J. Phys. Chem.* **1985**, *89*, 4495. (b) Howe, R. F.; Gratzel, M. *J. Phys. Chem.* **1987**, *91*, 3906.

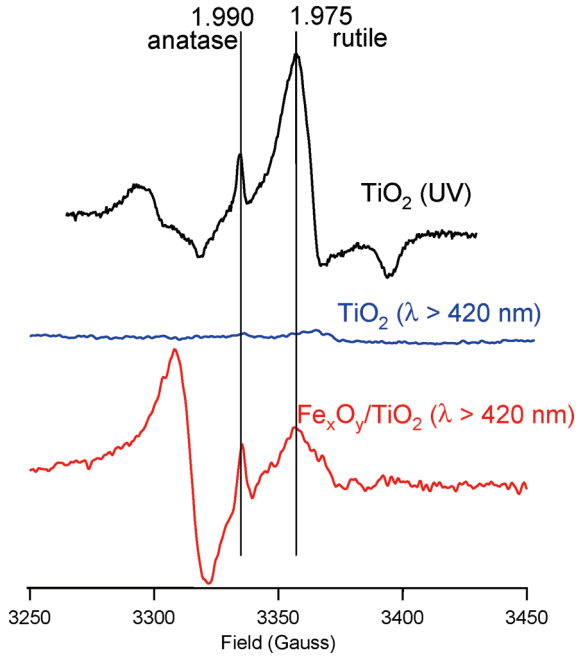

Figure 4. EPR spectra of bare TiO_2 and Fe_xO_y/TiO_2 nanocomposites measured at 4.5 K under visible light illumination (Xe-lamp, cut off filter 420 nm). For comparison, the spectrum of TiO_2 illuminated with UV light is also present.

associated with electrons in TiO_2 were observed upon illumination of a mixture of Fe_2O_3/TiO_2 with visible light. Although light energy is sufficient for photoexcitation of Fe_2O_3, the photogenerated electrons can not transfer from iron oxide to titania because the potential of conduction band edge of Fe_2O_3 (0.28 V) is >500 mV more positive than that of TiO_2 (−0.3 V). Therefore, nonstochiometric isolated Fe_xO_y clusters prepared by ALD onto titania surface promote the coupling of conduction band edges of mixed oxide, allowing transfer of photogenerated electrons from iron oxide to core titania. The nanocomposites thus exhibit novel photoelectrochemical properties: shift of absorption edge toward visible light as compared to TiO_2, and increased reducing power of photogenerated electrons as compared to Fe_2O_3.

The oxidation power of photogenerated holes in nanocomposites was investigated by following the formation of OH radicals. The formation of OH radicals upon UV excitation of aqueous TiO_2 is well established, and undergoes reaction of photogenerated holes with water molecules.[29−31] The reaction is thermodynamically favored because the potential of valence band holes of TiO_2 (2.8 V) is almost 1 V more positive than that of OH radicals (1.9 V). To examine possible formation of OH radicals upon excitation of Fe_xO_y/TiO_2, we have used a TEMPO free radical as a spin probe. The paramagnetic TEMPO nitroxide free radical undergoes reaction with OH radicals resulting in nonparamagnetic species,[32] and

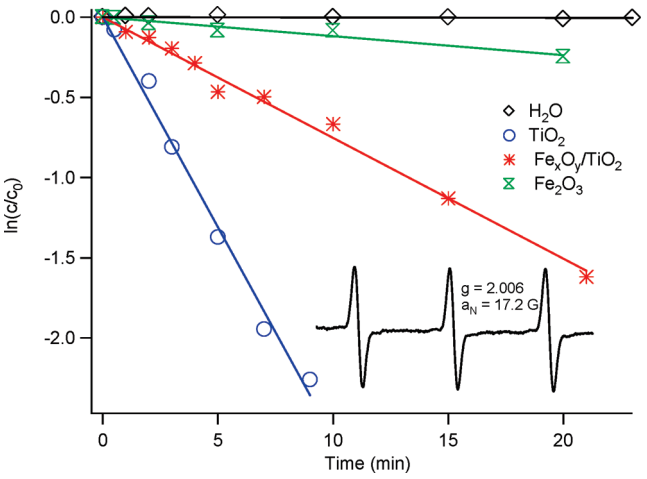

Figure 5. Relative changes of TEMPO free radical concentration upon UV/vis illumination (intensity 100 mW/cm^2). Inset: EPR spectrum of 20 μM TEMPO radical in the aqueous solution containing Fe_xO_y/TiO_2 before illumination. Typically, the sweep time for accumulation of a single spectrum was 42 s in all experiments.

thus the decrease in the intensity of its EPR spectrum correlates to the formed OH radicals.

The EPR spectrum of TEMPO radical presents a three-line signal characterized by $g = 2.006$ and hyperfine splitting $a_N = 17.2$ G, Figure 5 inset, and its photostability under UV light was confirmed previously.[31] The spectrum of TEMPO does not change in the presence of nanosomposites, indicating no preferential adsorption of radicals at their surfaces. The changes in TEMPO concentration over time were determined by measuring EPR spectra at certain time intervals, while solutions were under continuous UV/vis illumination. As can be seen from Figure 5, the rate of the formation of OH radicals is slower in the case of Fe_xO_y/TiO_2 nanocomposites as compared to bare titania, making nanocomposites less powerful oxidants. The UV photoexciatation of Fe_xO_y/TiO_2 can proceed through the excitation of electrons from the valence band of nanocomposite or from valence band of core TiO_2. Even if photoexcitation involves formation of photogenerated holes in core TiO_2, they will localize on the energetically preferential surface sites before reacting with surrounding water. In the case of nanocomposites these sites corresponds to Fe(III)-oxo centers on the surface of TiO_2. Thus Fe(III)-oxo centers on TiO_2 either change the valence band of nanocomposite material as a whole, or act as trapping sites lowering overall oxidation power under UV irradiation. Despite a smaller yield than for TiO_2, the formation of OH radicals from irradiated nanocomposites implies efficient charge separation. On the other hand, almost negligible formation of OH radicals was observed upon illumination of bare α-Fe_2O_3. Although this process is thermodynamically allowed (valence band edge 2.3 V), the short diffusion length of holes in ferric oxide restricts their reaction with adsorbed water molecules, the net result being charge recombination.

Photocatalytic Degradation of Methylene Blue under Visible Light. Finally, we have tested nanocomposites toward photodegradation of methylene blue (MB) under

(29) Hoffmann, M. R.; Martin, S. T.; Choi, W.; Bahnemann, D. W. *Chem. Rev.* **1995**, *95*, 69.
(30) Mills, A.; Le Hunte, S. *J. Photochem. Photobiol., A* **1997**, *108*, 1.
(31) Dimitrijevic, N. M.; Rozhkova, E.; Rajh, T. *J. Am. Chem. Soc.* **2009**, *131*, 2893.
(32) Brezova, V.; Dvoranova, D.; Stasko, A. *Res. Chem. Intermed.* **2007**, *33*, 251.

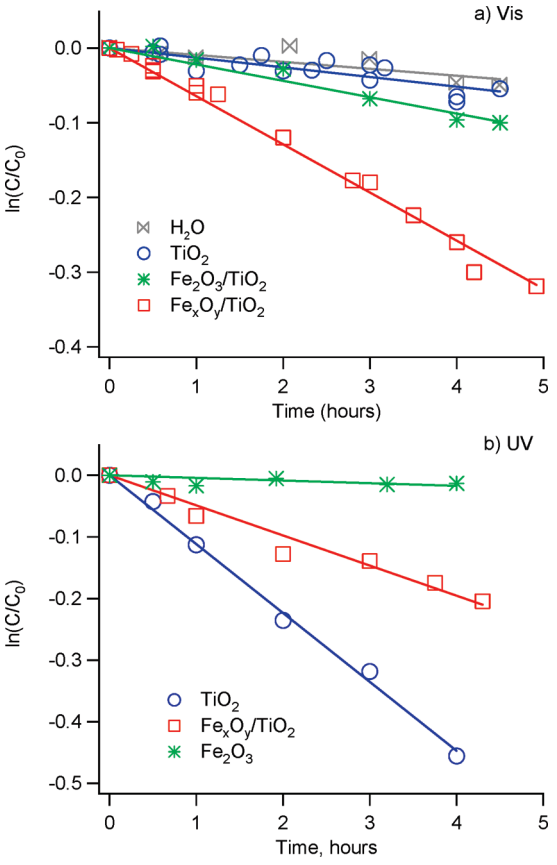

Figure 6. Relative concentration of methylene blue upon (a) visible (cut off filter 420 nm) and (b) UV (360 nm band-pass filter) light illumination of solutions containing 2 mg/mL of photocatalysts. The light intensity was 10 mW/cm^2.

visible light in order to confirm their novel photoelectrochemical properties. The well-established photobleaching of MB absorption involves both oxidative and reductive degradation.[33] The absorption of MB at 660 nm was monitored during the photodegradation process. Figure 6a plots the relative concentration of MB as a function of reaction time. Under the experimental conditions used in this study, the noteworthy degradation of MB was observed only for the ALD Fe_xO_y/TiO_2 nanocomposites, whereas both TiO_2 and a physical mixture of Fe_2O_3/TiO_2 did not contribute to MB decay to any significant extent under visible light. At the same time, a decrease in photocatalytic activity compared to bare P25 was observed under UV illumination, Figure 6b, and is probably due to the decrease in the overall oxidation power of nanocomposite, as was shown for the formation of OH radicals (Figure 5). However, the relative photocatalytic activity of Fe_xO_y/TiO_2 under UV light for formation of OH radicals is only ~30% of activity of bare P25, while for the degradation of methylene blue is ~50%. The oxidation potential of MB, $E^0(MB^+/MB) = 1.08$ V, is within the bang gap of nanocomposite. These results confirm that Fe_xO_y/TiO_2 nanocomposites can utilize both visible and UV light photocatalysis because of efficient charge separation, and unique redox properties of photogenerated charges. However, any doping that creates bulk or surface sites above the valence band edge of TiO_2 results in decreased UV-light photocatalytic activity compared to undoped TiO_2.[34]

In conclusion we have demonstrated that ALD allows the synthesis of small metal-oxide clusters, particularly Fe(III)-oxo centers, on the surface of TiO_2. The resulting nanocomposites have novel photoelectrochemical properties different from the core materials (both TiO_2 and Fe_2O_3), providing for efficient visible-light charge separation and photocatalysis.

Acknowledgment. The work was performed under the auspices of the U.S. Department of Energy, Office of Basic Energy Sciences, Division of Chemical Sciences, Geosciences and Biosciences, under Contract DE-AC02-06CH11357.

(33) Mills, A.; Wang, J. *J. Photochem. Photobiol., A* **1999**, *127*, 123.

(34) (a) Pore, V.; Heikkila, M.; Ritala, M.; Leskela, M.; Areva, S. *J. Photochem. Photobiol., A* **2006**, *177*, 68. (b) Pore, V.; Ritala, M.; Leskela, M.; Areva, S.; Jarn, M.; Jarnstrom, J. *J. Mater. Chem.* **2007**, *17*, 1361.